



Growth of new ternary intermetallic phases from Ca/Zn eutectic flux

Milorad Stojanovic, Susan E. Latturner*

Department of Chemistry and Biochemistry, Florida State University, Tallahassee, FL 32306-4390, USA

Received 10 August 2006; received in revised form 26 October 2006; accepted 14 December 2006

Abstract

The eutectic 7.3:2.7 molar ratio mixture of calcium and zinc metal melts at 394 °C and was explored as a solvent for the growth of new intermetallic phases for potential use as hydrogen storage materials. The reaction of nickel in this molten mixture produces two new phases—the CaCu₅-related structure CaNi₂Zn₃ (*P6/mmm*, *a* = 8.9814(5) Å, *c* = 4.0665(5) Å) and a new cubic structure Ca₂₁Ni₂Zn₃₆ (*Fd-3m*, *a* = 21.5051(4) Å). Palladium-containing reactions produced CaPd_{0.85}Zn_{1.15} with the orthorhombic TiNiSi structure type (*Pnma*, *a* = 7.1728(9) Å, *b* = 4.3949(5) Å, *c* = 7.7430(9) Å). Reactions of platinum in the Ca/Zn mixture produce Ca₆Pt₃Zn₅, with an orthorhombic structure related to that of W₃CoB₃ (*Pmmn*, *a* = 13.7339(9) Å, *b* = 4.3907(3) Å, *c* = 10.7894(7) Å).

© 2007 Published by Elsevier Inc.

Keywords: Flux; Calcium; Zinc; Eutectic; Intermetallic; Crystal; Nickel; Palladium; Platinum; Hydrogen storage

1. Introduction

A number of investigations have shown molten metal fluxes to be a powerful tool in materials synthesis [1,2]. The solubility of many reactants in molten metal renders them active at temperatures well below their melting point. Lower temperatures and the modified energetics in a flux allow for the isolation of complex metastable or kinetically stabilized phases, instead of the thermodynamic sinks (such as simple binary phases with highly stable structures) favored by high-temperature reactions. In contrast to the powders often obtained by conventional solid-state synthesis methods, the solution phase character of flux reactions promotes the growth of crystals, which are required for accurate structural and electronic characterization. A wide variety of metals have been used as solvents, with Sn, Ga, Al, and In being most common. Calcium has not been investigated as a flux due to its high melting point, volatility at high temperatures, and reactivity toward common crucible materials. We have found that the formation of a eutectic with zinc permits the use of calcium-rich solvents for intermetallic synthesis at tem-

peratures that minimize its volatility and reactivity toward reaction vessels.

Intermetallic compounds have come to the forefront as hydrogen storage materials due to their combination of high hydrogen capacity, close-to-ambient pressures and temperatures needed for activation, and the reversibility of the hydriding process [3]. These intermetallics are comprised of a very electropositive hydride-forming metal A (an element that will combine with H₂ to form a stable hydride, such as CaH₂) and a non-hydride forming metal B (a more electronegative transition metal that does not form a stable hydride). When these element classes are combined into an intermetallic phase, the resulting compound is often able to reversibly absorb hydrogen [4].

While LaNi₅ and other phases such as ZrMn₂ and YFe₃ have good hydrogen absorption kinetics, their high density is problematic. Investigations are needed to find other compounds with suitable absorption behavior that are comprised of lighter elements, and exploratory synthesis in flux mixtures is a promising avenue to investigate. Calcium and zinc are both relatively light metals; addition of an electronegative transition metal to a molten Ca/Zn eutectic mixture may result in formation of new intermetallic phases amenable to hydrogen absorption. Reactions of group 10 metals (Ni, Pd, Pt) in this eutectic has produced

*Corresponding author. Fax: +850 644 8281.

E-mail addresses: stojanovic@chem.fsu.edu (M. Stojanovic), lattur-
ne@chem.fsu.edu (S.E. Latturner).

1 the new phases CaNi_2Zn_3 , $\text{Ca}_{21}\text{Ni}_2\text{Zn}_{36}$, $\text{CaPd}_{0.85}\text{Zn}_{1.15}$,
 2 and $\text{Ca}_6\text{Pt}_3\text{Zn}_5$.

3 2. Experimental procedure

4 2.1. Synthesis

5 Reactants were used as received: Ca shot (99.5%, Alfa
 6 Aesar), Zn granules (99.8%, Alfa Aesar), Ni powder
 7 (99.9%, Strem Chemicals), Pt powder (99.9%, Alfa Aesar),
 8 and Pd powder (99.9%, Strem Chemicals). The initial
 9 reactant ratio was a 6:2:1 mmole ratio of Ca/Zn/(Ni, Pd, or
 10 Pt) elements. The reactants were placed into stainless-steel
 11 crucibles (5.8 cm length/0.9 cm diameter), with the calcium
 12 loaded last to allow it to melt and flow over the other
 13 reactants. The crucibles were then sealed into a fused silica
 14 tube under vacuum. The reaction was heated to 900 °C in
 15 6 h and was kept at this temperature for 12 h. Thereafter,
 16 the reaction was slowly cooled to 750 °C in 32 h, kept at
 17 750 °C for 36 h, cooled to 600 °C in 36 h, kept at 600 °C for
 18 12 h and cooled to room temperature in 48 h. After the
 19 cooling was finished, the crucible containing the reaction
 20 mixture was placed in water and sonicated for an hour to
 21 dissolve the excess calcium flux. The remaining product
 22 was washed with water and acetone and left to dry
 23 overnight. Gray powder and shiny gold-tinged metallic
 24 crystals were obtained. Occasionally, the crystals were
 25 coated with excess flux and they appeared gray. Repre-
 26 sentative yields of such reactions are 150 mg $\text{Ca}_{21}\text{Ni}_2\text{Zn}_{36}$
 27 and 60 mg of CaNi_2Zn_3 from reactions of 6:2:1 mmoles of
 28 Ca/Zn/Ni; 160 mg of $\text{CaPd}_{0.85}\text{Zn}_{1.15}$ from the Ca/Zn/Pd
 29 reaction, and 280 mg of $\text{Ca}_6\text{Pt}_3\text{Zn}_5$ from the Ca/Zn/Pt
 30 reaction.

31 Attempts to change the reactant ratio or scale up the
 32 reaction did not increase the yield. The ratios of 9:3:1.5 and
 33 12:4:2, respectively, were set up but the amount of product
 34 did not increase. Instead, more gray powder was obtained,
 35 and an increased attack on the quartz tubes was observed.
 36 The tubes are darkened and discolored after the normal
 37 scale reactions; if the amount of Ca is too high, the tubes
 38 will fail due to the increased amount of calcium vapor
 39 pressure. Isolation of the products by centrifugation was
 40 tried for the Ca/Ni/Zn system; the reaction was prepared in
 41 an identical way, but an iron screen (100 mesh) was placed
 42 on top of the loaded crucible and held in place by an empty
 43 crucible on top of it. The fused silica tube was then sealed
 44 under vacuum and heated using a program similar to the
 45 one described above. However, after the temperature was
 46 cooled to 600 °C, it was held at this temperature for 48 h,
 47 then cooled to 450 °C in 48 h. At this temperature, the tube
 48 was removed from the furnace, inverted, and centrifuged to
 49 force the excess molten Ca/Zn eutectic through the iron
 50 screen. The crystals isolated in the reaction crucible were
 51 slightly larger than those recovered through etching off the
 52 solidified flux.

53 Stoichiometric syntheses were also attempted by com-
 54 bining the elements in the ratios found in the flux-grown

55 crystalline products. Stainless-steel crucibles were used,
 56 with a solid steel ingot on top to limit volatilization of
 57 reactants; the heating profile was the same as that used for
 58 flux growth. The products were powders; they were mixed
 59 with silicon as an internal standard and were analyzed by
 60 powder X-ray diffraction. Only the CaPdZn phase was able
 61 to be obtained from a stoichiometric reaction (vide infra).
 62 The rest of the reactions yielded binary phases, predomi-
 63 nantly CaZn_2 and CaZn_3 .

64 2.2. Elemental analysis

65 Samples from each reaction were affixed to an aluminum
 66 SEM stub using carbon tape. Elemental analysis was
 67 performed on all samples using a JEOL 5900 scanning
 68 electron microscope with energy-dispersive X-ray spectro-
 69 scopy (EDXS) capabilities. Samples were analyzed using a
 70 30 kV accelerating voltage and an accumulation time of
 71 60 s. The EDXS analysis was fairly inconsistent and it
 72 depended on the amount of flux coating the crystals. Better
 73 results were obtained by cleaving the crystals and analyzing
 74 the inner surface. Representative Ca/X/Zn ratios of 35:5:60
 75 (for $\text{Ca}_{21}\text{Ni}_2\text{Zn}_{36}$), 20:30:50 (CaNi_2Zn_3), 35:30:35
 76 ($\text{CaPd}_{0.85}\text{Zn}_{1.15}$), and 45:15:40 ($\text{Ca}_6\text{Pt}_3\text{Zn}_5$) were observed.

77 2.3. X-ray diffraction

78 Single-crystal X-ray diffraction data was collected at
 79 room temperature using a Bruker AXS SMART CCD
 80 diffractometer with a Mo radiation source. Processing of
 81 the data was accomplished with use of the program
 82 SAINT; an absorption correction was applied to the data
 83 using the SADABS program. Refinement of the structure
 84 was performed using the SHELXTL package [5]. For the
 85 two Ca/Ni/Zn phases, nickel and zinc sites were difficult to
 86 distinguish in the X-ray data due to their similar electron
 87 density; non-calcium sites were initially refined as zinc and
 88 then nickel sites were assigned based on bond length
 89 arguments, comparison to other structures reported in the
 90 literature, and elemental analysis. Surprisingly, the *R*-
 91 values in both refinements did go down slightly when the
 92 Ni sites were assigned. In the final refinement cycle, the
 93 occupancies of Ni and Zn sites were allowed to vary to
 94 determine if mixed occupancy was present. The occupan-
 95 cies ranged from 0.98 to 1.01, but this does not rule out
 96 mixed occupancy (vide infra). Crystallographic parameters
 97 and atom position data for all four phases can be found in
 98 Tables 1–6. STRUCTURE TIDY was used to standardize
 99 the atomic coordinates [6].

100 Powder X-ray diffraction data was collected for the
 101 products of the stoichiometric reactions, as well as
 102 powdered products found in the flux reactions. Samples
 103 were analyzed using a Rigaku Ultima III powder
 104 diffractometer. The MDI JADE 7.0 X-ray pattern data
 105 processing software was used to determine which phases
 106 were present and calculate cell parameters.

Table 1
Crystallographic data collection parameters for Ca/X/Zn intermetallic phases

Compound	CaNi ₂ Zn ₃	Ca ₂₁ Ni ₂ Zn ₃₆	CaPd _{0.85} Zn _{1.15}	Ca ₆ Pt _{2.33} Zn _{5.67}
Formula weight	353.61	3312.42	204.94	1067.06
Space group	<i>P6/mmm</i>	<i>Fd-3m</i>	<i>Pnma</i>	<i>Pmnn</i>
<i>a</i> (Å)	8.9814(5)	21.5051(4)	7.1728(9)	4.3907(3)
<i>b</i> (Å)			4.3949(5)	13.7339(9)
<i>c</i> (Å)	4.0665(5)		7.7430(9)	10.7894(7)
<i>V</i> (Å ³)	284.08(4)	9945.4(3)	244.09(5)	650.62(4)
δ_{calc} (g/cm ³)	6.20	4.42	5.58	5.88
<i>Z</i>	3	8	4	2
Temperature (K)		298		
Radiation		MoK α		
Index ranges	$-11 \leq h, k \leq 11$ $-5 \leq l \leq 5$	$-28 \leq h, k, l \leq 28$	$-9 \leq h \leq 9$ $-5 \leq k \leq 5$ $-10 \leq l \leq 10$	$-5 \leq h \leq 5$ $-18 \leq k \leq 18$ $-14 \leq l \leq 14$
Absorption coeff. (mm ⁻¹)	29.6	19.9	19.1	43.5
Reflections collected	3844	32974	3056	8905
Unique data/parameters	172/20	638/38	342/21	950/50
<i>R</i> ₁ / <i>wR</i> ₂ (all data)*	0.0246/0.0576	0.0494/0.0879	0.0274/0.0673	0.0320/0.0657
Residual peak/hole (e ⁻ Å ⁻³)	0.954/-0.887	1.236/-1.865	1.43/-0.68	1.822/-2.483

$$R_1 = \frac{\sum \|F_o\| - |F_c|}{\sum \|F_o\|}; wR_2 = \frac{[\sum [w(F_o^2 - F_c^2)^2]]^{1/2}}{[\sum (wF_o^2)]^{1/2}}$$

Table 2
Atomic positions for CaNi₂Zn₃

Atom	Wyckoff site	<i>x</i>	<i>y</i>	<i>z</i>	<i>U</i> _{eq}
Ca1	1 <i>b</i>	0	0	1/2	0.0067(8)
Ca2	2 <i>c</i>	1/3	2/3	0	0.0066(6)
Ni1	6 <i>m</i>	0.1820(1)	0.3640(2)	1/2	0.0053(3)
Zn1	3 <i>g</i>	1/2	0	1/2	0.0066(4)
Zn2	6 <i>j</i>	0.2928(1)	0	0	0.0064(3)

*U*_{eq} is defined as one-third of the trace of the orthogonalized *U*_{ij} tensor.

Table 3
Atomic positions for Ca₂₁Ni₂Zn₃₆

Atom	Wyckoff site	<i>x</i>	<i>y</i>	<i>z</i>	<i>U</i> _{eq}
Ca1	96 <i>g</i>	0.06858(7)	0.06858(7)	0.3708(1)	0.0087(4)
Ca2	32 <i>e</i>	0.2165(1)	0.2165(1)	0.2165(1)	0.0066(7)
Ca3	8 <i>a</i>	1/8	1/8	1/8	0.005(1)
Ca4	32 <i>e</i>	0.4438(1)	0.4438(1)	0.4438(1)	0.0143(9)
Ni1	16 <i>c</i>	0	0	0	0.0049(7)
Zn1	96 <i>g</i>	0.28569(4)	0.28569(4)	0.10944(6)	0.0081(3)
Zn2	96 <i>g</i>	0.33332(4)	0.33332(4)	0.00711(6)	0.0083(3)
Zn3	96 <i>g</i>	0.32035(5)	0.32035(5)	0.22513(6)	0.0113(3)

*U*_{eq} is defined as one third of the trace of the orthogonalized *U*_{ij} tensor.

3. Results and discussion

A series of reactions were prepared in a 73% calcium/27% zinc eutectic mixture that melts at 394 °C [7]. This enabled much of the reaction heating to be carried out well below the melting point of Ca (842 °C), a temperature at which it is quite volatile and will degrade most crucible materials. All the Ca/M/Zn phases were obtained from the Ca/Zn flux as brittle, gold-tinged rounded blocks up to

Table 4
Selected bond lengths (in Å) in CaNi₂Zn₃ and Ca₂₁Ni₂Zn₃₆

CaNi ₂ Zn ₃		Ca ₂₁ Ni ₂ Zn ₃₆	
Ni–Zn1	2.4821(5) × 2	Ni–Zn1	2.592(1) × 6
Ni–Zn2	2.4839(3) × 4	Ni–Zn2	2.539(1) × 6
Ca1–Ni	2.831(1) × 6	Ca–Zn range	3.111(1)–3.315(2)
Ca2–Ni	3.1107(9) × 6	Ca–Ca1, Ca2, or Ca3 range	3.406(4)–3.486(4)
Ca1–Zn2	3.3245(8) × 6	Ca–Ca4 range	4.006(3)–4.185(4)
Ca2–Zn2	3.1912(6) × 6	Zn–Zn intericosahedral	2.635(2)–2.750(2)
Zn1–Zn2	2.7560(7) × 3	Zn2–Zn2 intricosahedral	2.535(3)
Zn2–Zn2	2.630(1) × 2	Zn3–Zn3 triangles	2.896(2)
		Zn1–Zn3	2.702(2)

Table 5
Atomic positions for CaPd_{0.85}Zn_{1.15}

Atom	Wyckoff site	<i>x</i>	<i>y</i>	<i>z</i>	Occ.	<i>U</i> _{eq}
Ca	4 <i>c</i>	0.0115(2)	1/4	0.6913(2)	1	0.0149(6)
Pd1/Zn1	4 <i>c</i>	0.2927(1)	1/4	0.3975(1)	0.85(3)/0.15(3)	0.0152(3)
Zn2	4 <i>c</i>	0.1654(2)	1/4	0.0766(1)	1	0.0167(4)

*U*_{eq} is defined as one third of the trace of the orthogonalized *U*_{ij} tensor.

1 mm in diameter. It is possible that the crystals were etched as the flux was being dissolved, resulting in the loss of visible external faceting; crystals isolated via centrifugation appear to be larger and better formed. The materials are stable in air for at least a month, but are dissolved in acid solutions and degrade slowly in water. The stainless-steel crucibles appeared to be inert to the reaction mixtures studied in this work; no iron incorporation was indicated in the elemental analysis, and no magnetic secondary phases were apparent when the products were probed with a magnet.

1 Table 6
 2 Atomic positions for $\text{Ca}_6\text{Pt}_{2.34}\text{Zn}_{5.66}$

3 Atom	Wyckoff site	x	y	z	Occ.	U_{eq}
5 Pt1/Zn1	4e	1/4	0.58568(3)	0.18499(4)	0.714(6)/0.286(6)	0.0112(2)
Pt2/Zn2	2a	1/4	1/4	0.43643(5)	0.909(7)/0.091(7)	0.0108(2)
7 Zn3	4e	1/4	0.00485(9)	0.7486(1)	1	0.0182(3)
Zn4	2b	1/4	3/4	0.0672(2)	1	0.0129(4)
Zn5	4e	1/4	0.08636(8)	0.3178(1)	1	0.0117(3)
9 Ca1	4e	1/4	0.1007(2)	0.0227(2)	1	0.0142(4)
Ca2	4e	1/4	0.6127(2)	0.4687(2)	1	0.0131(4)
11 Ca3	2b	1/4	3/4	0.7548(2)	1	0.0127(6)
Ca4	2a	1/4	1/4	0.7328(3)	1	0.0143(6)

13 U_{eq} is defined as one-third of the trace of the orthogonalized U_{ij} tensor.

15 3.1. CaNi_2Zn_3

17 This phase forms as the minority product (approx-
 19 imately 15% of the isolated solid) in syntheses with a 6:2:1
 Ca:Zn:Ni ratio. Other phases found in the products include
 21 $\text{Ca}_{21}\text{Ni}_2\text{Zn}_{36}$ (60% of the isolated product; vide infra),
 CaNi_2 (5%), CaZn_2 (15%), and CaZn_5 (5%); it is
 23 presumed that any more calcium-rich phases that might
 form in the synthesis are degraded during the etching away
 25 of the flux. The CaNi_2Zn_3 structure is related to the
 hexagonal CaCu_5 structure type observed for both CaZn_5
 27 and CaNi_5 ($a = 4.9516 \text{ \AA}$, $c = 3.9373 \text{ \AA}$ and $a = 5.405 \text{ \AA}$,
 $c = 4.183 \text{ \AA}$, respectively) [8]. However, ordering of nickel
 29 and zinc atoms on the transition metal sites produces a
 superstructure ($a^* = \sqrt{3}a$ and $c^* = c$) although the space
 31 group type remains the same ($P6/mmm$). The resulting unit
 cell parameters ($a^* = 8.9814(5) \text{ \AA}$, $c^* = 4.0665(5) \text{ \AA}$) fall in
 33 the range expected for a $\text{CaNi}_x\text{Zn}_{5-x}$ phase.

This ordered superstructure variant of the CaCu_5 type—
 35 the YCo_3Ga_2 structure type—is found in other phases such
 as GdNi_3Ga_2 and RENi_3Al_2 (RE = late rare-earth metal)
 37 [9]. Formation of the YCo_3Ga_2 form vs. the CaCu_5 form of
 a RE_3M_5 compound appears to be dependent on
 39 composition ($2 < x < 3$) and temperature. In several re-
 ported cases, inter-conversion between the two structure
 41 types is observed when annealing is carried out, indicating
 the CaCu_5 form is the high temperature structure type and
 43 the YCo_3Ga_2 variant is the low temperature structure type
 [10]. The ordering in CaNi_2Zn_3 results in the preferential
 45 location of nickel atoms on sites closest to the electro-
 positive calcium atoms, as would be expected from the
 47 higher electronegativity of nickel compared to zinc. As
 shown in Fig. 1, the Ca1 site is in a cylindrical environment
 49 with hexagonal symmetry, featuring $2.8310(9) \text{ \AA}$ bonds to
 six surrounding Ni atoms and $3.3245(6) \text{ \AA}$ distances to 12
 51 nearest zinc atoms. The short Ca1–Ni bonds are surprising,
 but they are similar to those observed in CaNi_2Si (2.862 \AA)
 53 and $\text{Ca}_3\text{Ni}_3\text{Si}_2$ (2.837 \AA , 2.852 \AA) [11]. The Ca2 site of
 CaNi_2Zn_3 has lower symmetry compared to the Ca1
 55 environment ($-6m2$ vs. $6/mmm$ site symmetry), but again
 features Ca–Ni distances ($3.111(2) \text{ \AA}$) that are shorter than
 57 the Ca–Zn distances ($3.1912(5) \text{ \AA}$). The nickel–zinc bonds

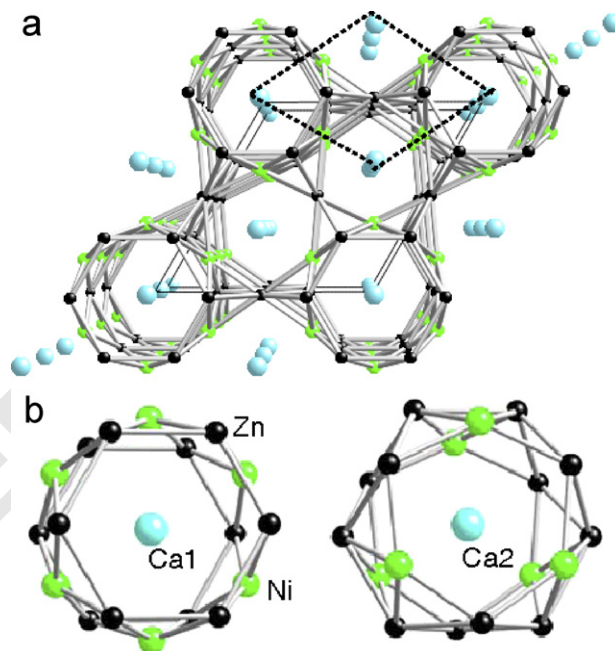


Fig. 1. (a) The CaNi_2Zn_3 structure type; the CaCu_5 substructure is indicated by a dashed unit cell. (b) The coordination environments of the two calcium sites in this structure.

fall in a very small range of $2.482\text{--}2.484 \text{ \AA}$; zinc–zinc bonds are longer, ranging from 2.63 to 2.76 \AA .

Because of the similarity in atomic number, Ni and Zn sites are difficult to distinguish in the X-ray structure solution. However, the formation of the YCo_3Ga_2 type supercell, and the distinct difference in the bond lengths to the Ni site compared to those to the Zn sites, support the idea that the CaNi_2Zn_3 compound is ordered. The occupancies of all five sites were allowed to vary in the last cycles of the refinement, but none of them varied significantly from one. Nevertheless, the possibility of Ni/Zn mixing on the non-calcium sites—producing a $\text{CaNi}_x\text{Zn}_{5-x}$ stoichiometric range—cannot be ruled out. Because this is a minority product in the flux reactions and could not be obtained through stoichiometric reaction, powder diffraction analysis of unit cell size was not possible. It should be noted that zinc doping of the CaNi_5

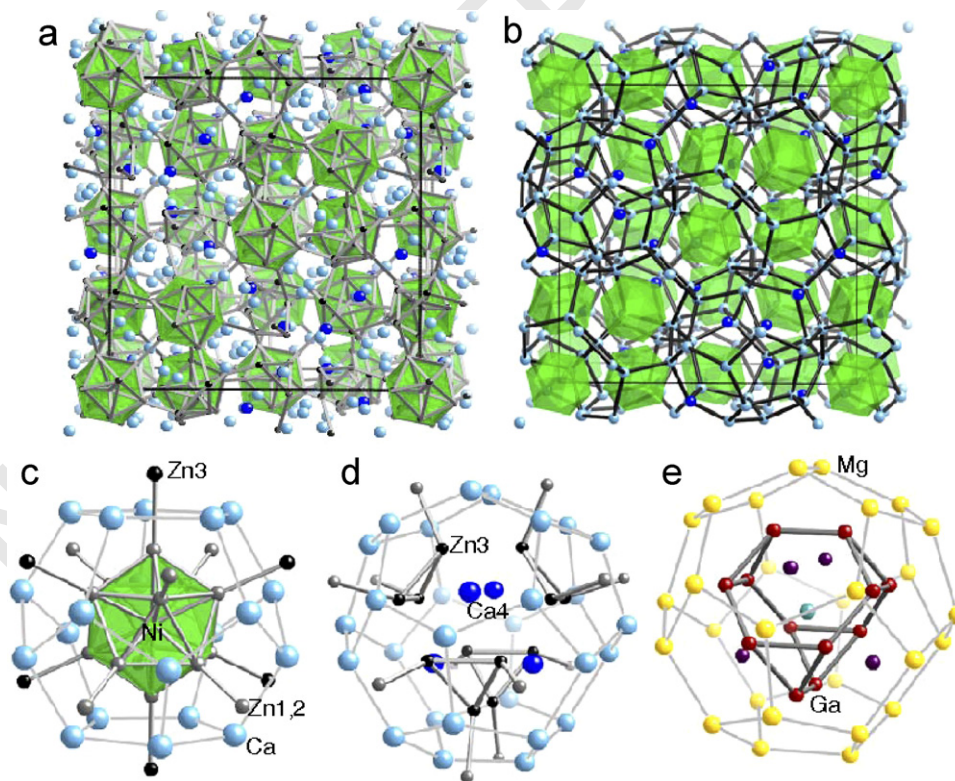
1 phase to modify its hydrogen absorption capabilities has
 2 been previously investigated. Ball milling and annealing
 3 were used to synthesize $\text{CaNi}_{4.7}\text{Zn}_{0.3}$. The unit cell
 4 parameters increased as expected ($a = 5.0165 \text{ \AA}$,
 5 $c = 3.9545 \text{ \AA}$), but no supercell formation or preferred
 6 siting was reported at this level of zinc substitution [12].

9 3.2. $\text{Ca}_{21}\text{Ni}_2\text{Zn}_{36}$

11 This phase forms as the majority product in syntheses
 12 with a 6:2:1 Ca:Zn:Ni ratio. This is a possibly new structure
 13 that demonstrates the icosagenic character of zinc. Other
 14 intermetallic structures containing zinc icosahedra centered
 15 with a transition metal include $\delta\text{-Co}_2\text{Zn}_{15}$, $\text{RT}_2\text{Zn}_{20}$
 16 ($T = \text{Fe, Ru, Co, Rh, Ni}$), and $\text{Zn}_{1-x}\text{Pd}_x$ [13]. In
 17 $\text{Ca}_{21}\text{Ni}_2\text{Zn}_{36}$, nickel-centered icosahedra (involving Ni1,
 18 Zn1, and Zn2; Ni–Zn bond lengths 2.539(1) and 2.592(1) \AA ;
 19 see Table 4) are linked together by the remaining zinc site
 20 (Zn3) to form a cubic unit cell shown in Fig. 2. The Zn–Zn
 21 bond lengths range between 2.63 and 2.75 \AA , similar to
 22 those in CaNi_2Zn_3 , with two exceptions. There is a shorter
 23 2.535(3) \AA Zn2–Zn2 bond linking together neighboring
 24 icosahedra; and the non-icosahedral Zn3 sites are linked to
 25 each other through a much longer bond of 2.896(2) \AA
 26 to form triangles.

27 The $\text{Ca}_{21}\text{Ni}_2\text{Zn}_{36}$ structure can be viewed as a zinc
 28 network defining icosahedral holes filled with Ni atoms and

29 larger sites filled with Ca atoms, but a more useful view is
 30 to consider the structure of the calcium network. This is a
 31 calcium-rich structure—three of the sites (Ca1, Ca2, and
 32 Ca3) are within a distance of 3.4–3.5 \AA to each other; the
 33 fourth Ca site (Ca4) is considerably further away from
 34 other Ca atoms (over 4 \AA) and is not considered a part of
 35 the calcium network. Linking together three of the calcium
 36 sites of $\text{Ca}_{21}\text{Ni}_2\text{Zn}_{36}$ results in a clathrate II type
 37 substructure (space group $Fd\bar{3}m$ (#227)). This makes
 38 $\text{Ca}_{21}\text{Ni}_2\text{Zn}_{36}$ a part of the family of cubic compounds
 39 which have a clathrate II arrangement of alkali metal and/
 40 or alkaline earth metals surrounding a variety of anionic
 41 clusters. This is the first member of this class to have a zinc-
 42 rich stoichiometry. Previous examples of this family
 43 contain a preponderance of group 13 elements and include
 44 $\text{K}_{17}\text{In}_{41}$, $\text{K}_{39}\text{In}_{80}$, $\text{Na}_{22}\text{Ga}_{39}$, $\text{Na}_{35}\text{Cd}_{24}\text{Ga}_{56}$, $\text{K}_{14}\text{Na}_{20}$
 45 $\text{In}_{91.818}\text{Li}_{13.182}$ and $\text{Mg}_{35}\text{Cu}_{24}\text{Ga}_{53}$ [14,15]. In these struc-
 46 tures, linking the electropositive metals together will form
 47 the pentagonal dodecahedra (a 20 atom polyhedron, A_{20})
 48 and hexakaidecahedra (a 28 atom polyhedron, A_{28}) of the
 49 clathrate II structure. The $\text{Ni}@Zn_{12}$ icosahedra of Ca_{21} -
 50 $\text{Ni}_2\text{Zn}_{36}$ are encased in the pentagonal dodecahedra of
 51 calcium atoms. The larger tetrahedrally symmetric hex-
 52 akaidecahedra formed by Ca1, Ca2, and Ca3 atoms
 53 contain the Zn3 and Ca4 sites. As shown in Fig. 2d, the
 54 four hexagonal windows of this polyhedron are adjacent to
 55 the four Ca4 atoms. Each of the pentagonal windows is



56 Fig. 2. The $\text{Ca}_{21}\text{Ni}_2\text{Zn}_{36}$ structure type: (a) view highlighting the linkages between the nickel centered icosahedra and additional zinc sites; calcium atoms
 57 are shown as non-bonded spheres, (b) view highlighting the clathrate II framework produced by connecting 3 of the calcium sites, (c) the pentagonal
 58 dodecahedron of calcium sites, encapsulating the $\text{Ni}@Zn_{12}$ icosahedron, (d) the hexakaidecahedron of calcium sites, encapsulating the triangles of Zn3
 59 atoms and the Ca4 site and (e) a comparison to the contents of the Mg_{26} hexakaidecahedron of $\text{Mg}_{35}\text{Cu}_{24}\text{Ga}_{53}$.

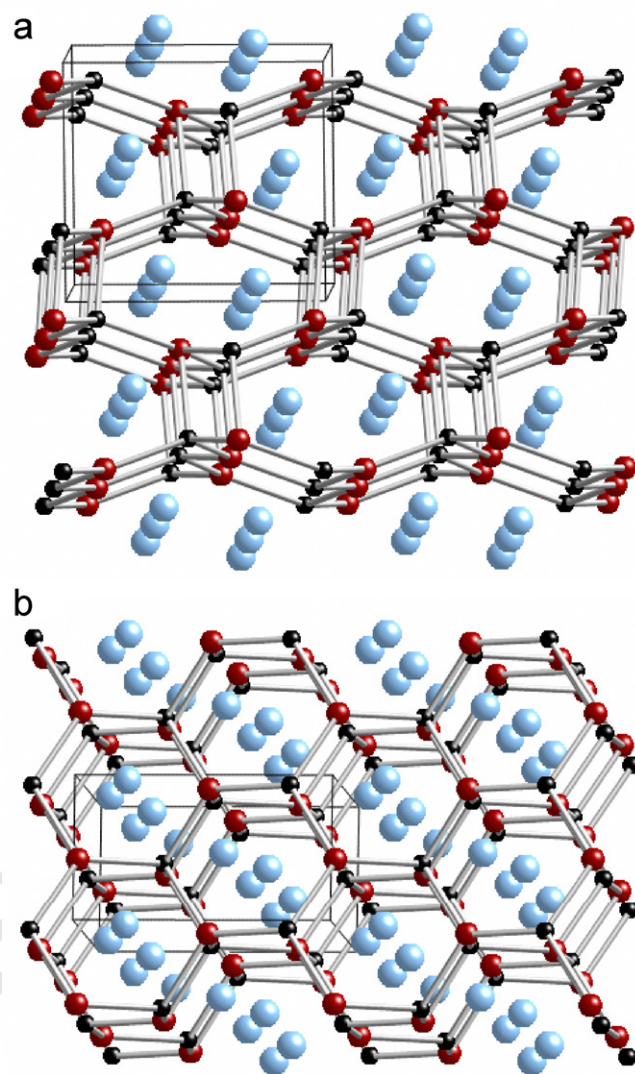
1 capped by a Zn3 site; these zinc atoms are close enough to
 2 each other to form weak Zn3–Zn3 bonds, resulting in
 3 triangles.

4 The $\text{Ca}_{21}\text{Ni}_2\text{Zn}_{36}$ structure bears a strong resemblance to
 5 that of $\text{Mg}_{35}\text{Cu}_{24}\text{Ga}_{53}$ —comprised of a Mg clathrate II
 6 network surrounding linked anionic Cu/Ga clusters—with
 7 a number of small differences.¹⁵ The nickel-centered
 8 $\text{Ni}@\text{Zn}_{12}$ icosahedra in $\text{Ca}_{21}\text{Ni}_2\text{Zn}_{36}$ are paralleled by
 9 empty Cu_6Ga_6 icosahedra in the gallide phase. Conversely,
 10 the cluster within the A_{28} hexakaidecahedra is centered by
 11 a Mg atom in $\text{Mg}_{35}\text{Cu}_{24}\text{Ga}_{53}$ and it is empty in the
 12 compound studied in this work (Figs. 2d and 2e). The
 13 $\text{Mg}@\text{Ga}_{16}$ cluster is described as an icosioctahedron,
 14 generated by linking together 12 Ga atoms (four triangles
 15 of Ga connected to form a truncated tetrahedron) and
 16 capping the four hexagonal faces with additional Ga sites.
 17 This parallels the four triangles of Zn3 seen in Ca_{21} -
 18 $\text{Ni}_2\text{Zn}_{36}$, but these triangles are not close enough to form
 19 bonds between them (Zn3–Zn3 bonds within triangles are
 20 2.896 Å; between triangles, the Zn–Zn distance is 3.324 Å).
 21 The Ga sites capping the hexagonal faces in the $\text{Mg}@\text{Ga}_{16}$
 22 cluster are replaced by Ca4 atoms in the structure studied
 23 here.

24 As in the case of CaNi_2Zn_3 , mixing of Ni/Zn on the non-
 25 calcium sites of the $\text{Ca}_{21}\text{Ni}_2\text{Zn}_{36}$ structure cannot be ruled
 26 out. Nickel and zinc sites were assigned based on bond
 27 lengths and comparison to features of known structures
 28 (such as the $\text{Ni}@\text{Zn}_{12}$ icosahedron in the $\text{TNi}_2\text{Zn}_{20}$
 29 phases). Again, the Ni–Zn bond lengths are shorter than
 30 the Zn–Zn bond lengths for the most part. A number of
 31 different crystals of the $\text{Ca}_{21}\text{Ni}_2\text{Zn}_{36}$ phase, synthesized
 32 in different reactions with different reactant ratios, were
 33 screened on the single-crystal diffractometer; the unit cell
 34 parameter did not vary greatly ($a = 21.505(8)–21.513(9)\text{Å}$).
 35 This compound could not be synthesized by stoichiometric
 36 combination of the elements, but powder diffraction of flux
 37 reaction products indicated a unit cell of $a = 21.53(2)\text{Å}$,
 38 only slightly larger than those shown in the single-crystal
 39 data. This small observed range supports the idea that this
 40 phase is most likely highly ordered.

41 3.3. $\text{CaPd}_{0.85}\text{Zn}_{1.15}$

42 The only ternary phase resulting from the combination
 43 of Ca, Pd, and Zn is the roughly 1:1:1 stoichiometry
 44 compound with the orthorhombic TiNiSi structure. This is
 45 a common structure type for intermetallics containing
 46 equimolar amounts of an electropositive element, a heavy
 47 late transition metal, and a main group element; analogs
 48 include HoIrSi , CaAuIn , and EuPtIn [16,17]. The Zn
 49 atoms in CaPdZn are tetrahedrally coordinated by four Pd
 50 atoms, with Zn–Pd bonds in the 2.6–2.7 Å range. The Pd
 51 atoms are also 4 coordinate, but in a less symmetric
 52 fashion. This can be considered a distortion of the
 53 hexagonal AlB_2 parent structure, a relationship that
 54 becomes evident upon viewing the structure down the a -
 55 axis (see Fig. 3) [18]. This structure type does allow for
 56



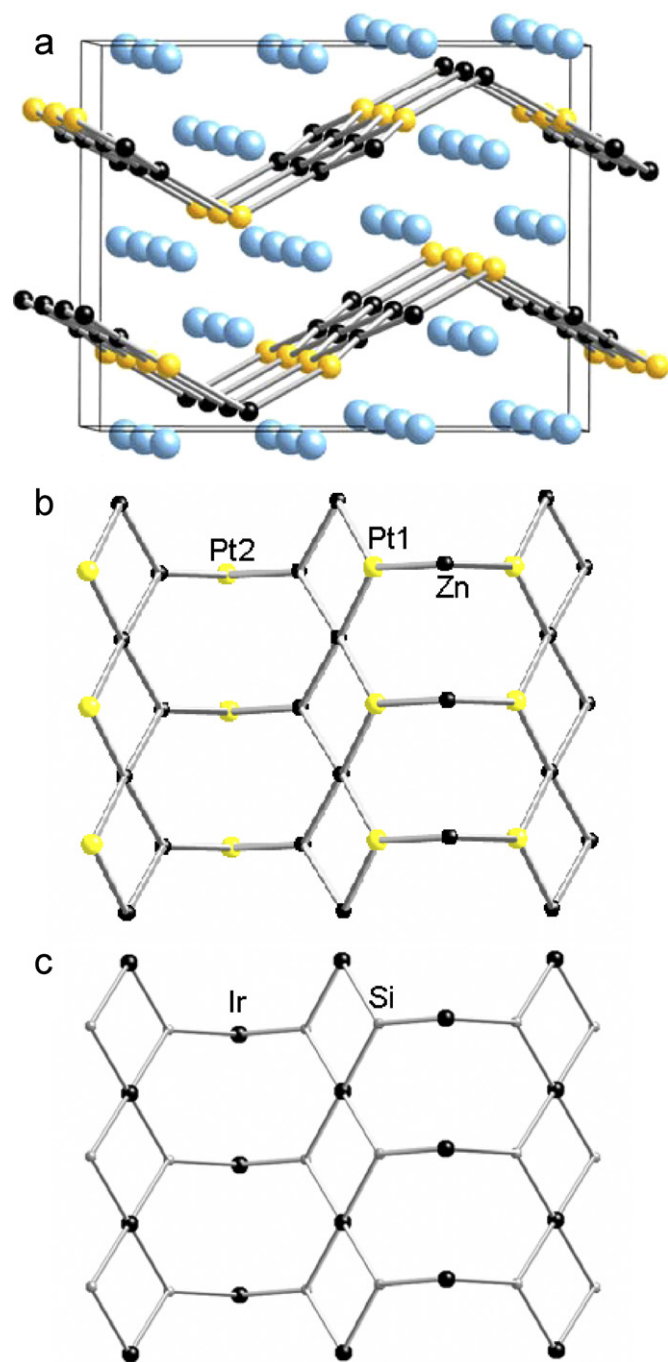
57 Fig. 3. The CaPdZn structure (TiNiSi structure type). Large blue spheres
 58 are Ca; small red spheres are Pd; small black spheres are Zn atoms: (a)
 59 view down the b -axis and (b) view down the a -axis, highlighting the
 60 relationship to the AlB_2 structure type.

61 some solid solution, and Pd/Zn mixing is observed on the
 62 Pd site. An attempt to synthesize this compound from a
 63 1:1:1 ratio of elements proved successful, yielding a poorly
 64 crystalline phase with orthorhombic unit cell parameters of
 65 $a = 7.136(7)\text{Å}$, $b = 4.421(5)\text{Å}$, $c = 7.755(9)\text{Å}$. The intensi-
 66 ties of the peaks in the powder pattern match those
 67 calculated for CaPdZn using CrystalDiffract [19].

68 3.4. $\text{Ca}_6\text{Pt}_3\text{Zn}_5$

69 This ternary phase was obtained in low yield (30%,
 70 based on amount of Pt used), with CaZn_2 being the other
 71 predominant phase isolated in the synthesis. This com-
 72 pound forms in an orthorhombic structure type (space
 73 group $Pmmn$) that is a new variant of the structure of
 74 W_3CoB_3 and $\text{Sm}_3\text{Ir}_2\text{Si}_2$ [11,17]. Both of these compounds
 75 have $Cmcm$ symmetry, with unit cell parameters similar
 76 to $\text{Ca}_6\text{Pt}_3\text{Zn}_5$ (for $\text{Sm}_3\text{Ir}_2\text{Si}_2$, $a = 4.0969(2)\text{Å}$, $b =$

1 10.5932(7)Å; $c = 13.2753(8)$ Å). The atomic locations are
 2 identical; the symmetry lowering is due to the variation in
 3 ordering of the atoms on the crystallographic sites in the
 4 unit cell. The puckered Pt/Zn sheets in Fig. 4b correspond
 5 to the CoB_3 sheets in W_3CoB_3 and the Ir_2Si_2 sheets in
 6 $\text{Sm}_3\text{Ir}_2\text{Si}_2$. Compared to the puckered Ir/Si sheet (shown in
 7 Fig. 4c), the pattern of site occupancy seen in $\text{Ca}_6\text{Pt}_3\text{Zn}_5$
 8 results in loss of local symmetry elements such as mirror



9
11
13
15
17
19
21
23
25
27
29
31
33
35
37
39
41
43
45
47
49
51
53
55
57
Fig. 4. The $\text{Ca}_6\text{Pt}_3\text{Zn}_5$ structure: (a) view down the b -axis, showing the
 puckered sheets formed by the Pt and Zn sites, (b) an individual sheet
 viewed down the c -axis, showing the distribution of Pt and Zn and (c)
 comparison to the higher symmetry Ir/Si puckered sheet of $\text{Sm}_3\text{Ir}_2\text{Si}_2$.

planes and inversion centers, causing a lowering of the
 overall space group symmetry from $Cmcm$ to $Pmnn$.

The late transition metals in $\text{Sm}_3\text{Ir}_2\text{Si}_2$ and W_3CoB_3
 occupy the square planar site in the puckered layers of this
 structure; it is somewhat surprising that the platinum
 atoms in $\text{Ca}_6\text{Pt}_3\text{Zn}_5$ do not. Both of the platinum sites are
 partially occupied by zinc atoms (resulting in an actual
 stoichiometry of $\text{Ca}_6\text{Pt}_{2.34}\text{Zn}_{5.66}$), but there does not
 appear to be any evidence of platinum mixing into the
 square planar zinc site. The siting of platinum may be
 directed by promotion of short Pt–Ca distances; the Pt sites
 are within 3.0–3.2 Å of several calcium atoms. The zinc
 sites are further away from the calcium atoms on average.
 As in the case of CaNi_2Zn_3 , the favorable interaction
 between the relatively electronegative transition metal
 atoms and the electropositive calcium atoms may stabilize
 the ordering of atoms in the structure. Band structure
 calculations are needed to further investigate this aspect of
 these phases.

4. Conclusion

Ca/Zn eutectic has proven to be a useful synthesis media
 for new intermetallic phases. Addition of group 10
 transition metals to this flux results in the formation of
 new materials. Initial investigations into replacing Ni, Pd,
 and Pt with other transition metals (including Fe, Ru, Au,
 Ag, Mn) have proven unsuccessful thus far, yielding either
 CaZn_2 and unreacted transition metals, or known binary
 phases such as CaAg_2 . Experiments are underway to
 explore additional reactants and to investigate the hydro-
 gen storage and catalytic properties of the compounds
 synthesized in this work.

Acknowledgments

This research made use of the Scanning Electron
 Microscope facilities of MARTECH at Florida State
 University. Financial support from the NSF (Grant
 DMR-05-47791), the ACS Petroleum Research Fund,
 and an ORAU Ralph E. Powe Award is gratefully
 acknowledged. We thank J. Corbett, B. Li, and Q. Lin
 for useful discussions.

Appendix A

Additional details regarding the crystallographic refine-
 ments can be obtained from the Fachsinformationszentrum
 Karlsruhe, 76344 Eggenstein-Leopoldshafen, Germany (e-
 mail: www.crysdata@fiz.karlsruhe.de) on quoting the
 depository numbers 417124 ($\text{Ca}_6\text{Pt}_3\text{Zn}_5$), 417125
 ($\text{CaPd}_{0.85}\text{Zn}_{1.15}$), 417126 (CaNi_2Zn_3), and 417127 (Ca_{21} -
 $\text{Ni}_2\text{Zn}_{36}$).

1 **References**

- 3 [1] Z. Fisk, J.P. Remeika, in: Gschneider, Eyring (Eds.), Handbook on
 5 the Physics and Chemistry of Rare Earths, Vol. 12, Elsevier Science,
 Amsterdam, 1989 (Chapter 81);
 Z. Fisk, P.C. Canfield, *Phil. Mag.* 65 (1992) 1117–1123.
- 7 [2] M.G. Kanatzidis, R. Pöttgen, W. Jeitschko, *Angew. Chem. Int. Ed.*
 44 (2005) 6996–7023.
- 9 [3] A. Zuttel, *Naturwissenschaften* 91 (2004) 157–172;
 G. Sandrock, *J. Alloy Compd.* 293–295 (1999) 877–888.
- 11 [4] M. Morinaga, H. Yukawa, K. Nakatsuka, M. Takagi, *J. Alloy*
 13 *Compd.* 330–332 (2002) 20–24.
- 15 [5] SAINT, version 6.02a, Bruker AXS Inc., Madison, WI, 2000.;
 G.M. Sheldrick, SHELXTL NT/2000, version 6.1, Bruker AXS Inc.,
 17 Madison, WI, 2000.
- [6] L.M. Gelato, E. Parthe, *J. Appl. Crystallogr.* 20 (1987) 139–143.
- [7] T.B. Massalski, H. Okamoto, *Binary Alloy Phase Diagrams*, second
 ed., ASM International, Materials Park, OH, 1990.
- [8] P. Villars, L.D. Calvert, *Pearson's Handbook—Crystallographic*
 17 *Data for Intermetallic Phases*, ASM International, Materials Park,
 OH, 1998.
- 19 [9] M.A. Fremy, D. Gignoux, J.M. Moreau, D. Paccard, I. Paccard, *J.*
 21 *Less-Common Met.* 106 (1985) 251–255;
 B. Šorgić, A. Drašner, Ž. Blažina, *J. Alloy Compd.* 356–357 (2003)
 23 501–504;
 Ž. Blažina, B. Šorgić, A. Drašner, *J. Phys.: Condens. Matter* 11
 25 (1999) 3105–3114.
- [10] H. Flandorfer, P. Rogl, K. Hiebl, E. Bauer, A. Lindbaum, E. Gratz,
 C. Godart, D. Gignoux, D. Schmitt, *Phys. Rev. B* 50 (1994)
 15527–15541; 27
 A. Drašner, Ž. Blažina, *J. Alloy Compd.* 359 (2003) 180–185. 29
- [11] J. Glaser, *Z. Anorg. Allg. Chem.* 628 (2002) 1946–1950.
- [12] G. Liang, J. Huot, R. Schulz, *J. Alloy Compd.* 321 (2001) 146–150. 31
- [13] M. Böstrom, S. Lidin, *J. Solid State Chem.* 166 (2002) 53–57;
 T. Nasch, W. Jeitschko, U.C. Rodewald, *Z. Naturforsch. B* 52 (1997)
 1023–1030; 33
 O. Gourdon, Z. Izaola, L. Elcoro, V. Petricek, G.J. Miller, *Phil. Mag.*
 86 (2006) 419–425. 35
- [14] B. Li, J.D. Corbett, *J. Am. Chem. Soc.* 127 (2005) 926–932; 37
 G. Cordier, V. Müller, *Z. Naturforsch. B.* 49 (1994) 721;
 B. Lin, J.D. Corbett, *Inorg. Chem.* 42 (2003) 8768;
 M. Tillard-Charbonnel, N. Chouaibi, C. Belin, *Mater. Res. Bull.* 27
 (1992) 1277. 39
- [15] Q. Lin, J.D. Corbett, *Inorg. Chem.* 44 (2005) 512–518.
- [16] D. Kußmann, R. Hoffmann, R. Pöttgen, *Z. Anorg. Allg. Chem.* 624
 (1998) 1727–1735; 41
 R. Pottgen, *Z. Kristallogr.* 211 (1996) 884–890.
- [17] R. Mishra, R. Hoffmann, R. Pöttgen, *Z. Anorg. Allg. Chem.* 627
 (2001) 1787–1792. 43
- [18] R.D. Hoffmann, R. Pöttgen, *Z. Kristallogr.* 216 (2001) 127–145. 45
- [19] CrystalDiffract, version 1.0.2. M. Conley, D. Palmer, CrystalMaker
 Software Ltd., Oxfordshire, UK, 1994–2006. 47